INTERNATIONAL ATOMIC ENERGY AGENCY
UNITED NATIONS EDUCATIONAL, SCIENTIFIC AND CULTURAL ORGANIZATION

INTERNATIONAL CENTRE FOR THEORETICAL PHYSICS
34100 TRIESTE (ITALY) - P.O.B. 586 - MIRAMARE - STRADA COSTIERA 11 - TELEPHONE: 2240-1
CABLE: CENTRATOM - TELEX 460392-1

SMR/291 - 46

SPRING COLLEGE IN CONDENSED MATTER
ON
"THE INTERACTION OF ATOMS & MOLECULES WITH SOLID SURFACES"
(25 April - 17 June 1988)

REACTIONS ON SURFACES AND CATALYSIS
(Lectures I, II & III)

David W. GOODMAN
Surface Science Division
Sandia National Laboratories
Albuquerque, New Mexico 87185
U.S.A.

Correlations Between Surface Structure and Catalytic Properties: Structure-insensitive Reactions
I. Methanation

D. W. Goodman
Surface Science Division
Sandia National Laboratories
Albuquerque, NM 87185

ABSTRACT

Recent work has demonstrated the special advantages of meshing in a single apparatus kinetic measurements at process-like conditions with modern surface analytical techniques for fundamental catalytic studies. These data have shown that low surface area monolithic materials can be used successfully to model certain catalytic systems. Virtually identical kinetic parameters have been found for the methanation reaction over single crystals of nickel and ruthenium as have been measured for high surface area nickel and ruthenium supported catalysts. Furthermore, surface probes have allowed the methanation reaction to be dissected mechanistically in that the kinetics associated with the two major reaction steps have been measured individually.

The methanation reaction [1,2] (Reaction 1) has a critical

$$3H_2 + CO \text{ ----> } CH_4 + H_2O \qquad (1)$$

role in the production of synthetic natural gas from hydrogen-deficient carbonaceous materials. In addition, this reaction is an obvious starting point in studies of fuel and chemical synthesis from carbon sources. Historically this reaction has been considered to be structure insensitive [1] in that changes in catalyst morphology generally produce, at most, small changes in the catalytic activity. Because of this and the extensive work addressing the chemisorptive properties of H_2 and CO in ultrahigh vacuum (UHV) surface science studies, methanation has proved to be an ideal reaction for model catalytic studies combining surface analytical techniques with reaction kinetics [3].

The studies to be discussed were carried out utilizing the specialized apparatus shown in Figure 1 and described in references [3,4]. This device consists of two distinct regions, a surface analysis chamber and a microcatalytic reactor. The custom built reactor, contiguous to the surface analysis chamber, employs a retraction bellows that supports the metal single crystal and allows translation of the catalyst in vacuo from the reactor to the surface analysis region. Both regions are of ultrahigh vacuum construction, bakeable, and capable of ultimate pressures of less than 2×10^{-10} Torr. Auger spectroscopy (AES) is used to characterize the sample before and after reaction. A second chamber was equipped with Auger spectroscopy, low energy electron diffraction (LEED) and a mass spectrometer for temperature programmed desorption (TPD).

For methanation on nickel it has been possible to correlate kinetic parameters with those found for supported high-area catalysts [2,3]. The data in the Arrhenius plot of Fig. 2a represent steady-state, specific methanation rates on both the Ni(111) and Ni(100) surfaces [5]. The atomic configurations of the Ni(100) and Ni(111) surfaces are shown in figures 2b and 2c, respectively. The similarity between the close-packed (111) and the more open (100) crystal plane of Ni is evident in both the value of the specific rates and activation energy (103 kJ/mole). In the temperature range of 450-700K, methane production rates vary by almost five orders of magnitude. It should be pointed out that measurements over such a wide temperature range are difficult, if not impossible, with supported high surface area catalysts due to heat and mass transfer limitations at high temperatures.

The single crystal results are compared in Fig. 2 with three sets of data taken from Ref. [5] for nickel supported on alumina, a high surface area catalyst. This comparison shows extraordinary similarities in kinetic data taken under nearly identical conditions. Thus, for the H_2-CO reaction over nickel, there is no significant variation in the specific reaction rates or the activation energy as the catalyst changes from small metal particles to bulk single crystals. These data provide convincing evidence that the methanation reaction rate is indeed structure insensitive on nickel catalysts.

For the methanation reaction surface characterization subsequent to reaction has provided data addressing the reaction

mechanism. Auger spectroscopic analysis of an active nickel catalyst following reaction at atmospheric pressure [2,3] has been accomplished by evacuating the reactor and transferring the crystal to the surface analysis chamber. Auger analysis after such a procedure shows a carbonaceous species present on the surface at a concentration equivalent to approximately 10% of a monolayer, (a monolayer (ML) in this context is defined as one atom per one substrate metal atom). The AES spectrum shown in Fig. 3c indicates this carbon to be a "carbidic" form with a lineshape distinctive from that of graphitic carbon [3,4] shown in Fig. 3b. This carbidic-type carbon can be readily removed by heating the crystal to 600K in atmospheric H_2, with the product formed being methane. A carbon species with these same characteristics can be produced by heating the Ni crystal in CO in the absence of hydrogen. Figure 3 shows the AES carbon signal [3] measured after heating a Ni(100) crystal in several Torr of CO at 600K [Fig. 3c] and at 700K [Fig. 3a]. These carbon peaks are compared with those observed with single crystal graphite [Fig. 3b] and with bulk nickel carbide [Fig. 3d]. Based on this comparison, the active carbon form has been designated "carbidic". The deposition of an active carbon and the absence of oxygen on the nickel surface following heating in pure CO is consistent with a well-known disproportionation reaction, the Boudouard reaction,

$$2CO \longrightarrow C + CO_2$$

which has been studied on supported Ni catalysts [7,8] and on Ni films [9]. Studies such as those described here show that methane can be catalytically synthesized over Ni by an active

(carbidic) carbon formed via the Boudouard reaction and its subsequent hydrogenation to methane. However, to demonstrate that this surface carbon route is the major reaction pathway, kinetic measurements of both carbon formation from CO and its removal by H_2 were carried out [10].

In the first set of measurements [10] the rate of carbon build-up on a Ni(100) surface was measured at various temperatures as follows: (1) surface cleanliness was established by AES (2) the sample was retracted into the reaction chamber and exposed to several Torr of CO for various times at a given temperature (3) after evacuation the sample was transferred to the analysis chamber and (4) the AES spectra of C and Ni were measured. Two features of this study are noteworthy. First, two kinds of carbon forms are evident - a carbidic type which occurs at temperatures < 650K and a graphite type at temperatures > 650K. The carbide form saturates at 0.5 monolayers. Second, the carbon formation data from CO disproportionation indicates a rate equivalent to that observed for methane formation in a H_2/CO mixture. Therefore, the surface carbon route to product is sufficiently rapid to account for methane production with the assumption that kinetic limitations are not imposed by the hydrogenation of this surface carbon.

A second set of experiments [10] further supported the surface carbon route to methane. In these experiments a Ni(100) surface was precarbided by exposure to CO and then treated with hydrogen in the reaction chamber for various times. Steps (3) and (4) above were then followed to measure the carbide level.

This study showed that the rate of carbon removal in hydrogen compared favorably to the carbide formation rate in CO and to the overall methanation rate in H_2/CO mixtures. Thus in a H_2-CO atmosphere the reaction rate is determined by a delicate balance of the carbon formation and removal steps and neither of these is rate determining in the usual sense.

According to this mechanism, if the surface coverage of atomic hydrogen is close to saturation, it is predicted that (a) further increases in hydrogen pressure would have almost no effect on the methane rate and (b) a low surface carbon level will result. This is the condition believed to exist under the reaction conditions of Fig. 2a. However, if reaction conditions are altered such that the surface hydrogen concentration decreases (e.g. low H_2 pressure and high temperature) then the mechanism demands a correlation of decreasing methane yield with increasing surface carbide. This correlation between the rate of production of methane and the steady-state surface carbide concentration holds very well as evidenced by the data in Fig. 4 [5]. Here all reaction rate data measured over a Ni(100) catalyst at 625 K lie on a smooth curve when plotted against the measured steady-state carbide level, regardless of H_2/CO ratio or total pressure.

Thus, the proposed reaction mechanism involving the dissociation of CO and the subsequent hydrogenation of the resulting carbon species (C_{ads}) accounts quite satisfactorily for the effect of pressure on the methanation rate, for the variation in the measured surface carbon level as reaction parameters are changed, and for the formation at a characteristic temperature

and pressure conditions of a catalyst-deactivating graphitic carbon. Recent studies [11] using isotopically labelled CO have shown that the CO dissociation step is essentially unidirectional in that the rate of C_{ads} and O_{ads} recombination is insignificantly slow compared to the C_{ads} hydrogenation rate.

Methanation reactions over Ni, Ru, [5,12], and Fe [13] show remarkable similarities in many critical parameters suggesting that the three metals behave essentially the same catalytically. This conclusion finds support in studies with nickel, ruthenium, and cobalt high-surface-area supported catalysts [7,8,14,15] and with studies using Ni, Co, and Ru films in UHV [16].

ACKNOWLEDGEMENT

We acknowledge with pleasure the partial support of this work by the Department of Energy, Office of Basic Energy Sciences, Division of Chemical Sciences.

REFERENCES

1. M. A. Vannice, Catal. Rev., 14, 153 (1976).
2. Kelley, R. D.; Goodman, D. W., The Chemical Physics of Solid Surfaces and Heterogeneous Catalysts, Vol.4, Elsevier, 1982.
3. D. W. Goodman, R. D. Kelley, T. E. Madey and J. T. Yates, Jr., J. Catal., 63, 226 (1980).
4. D. W. Goodman, Ann. Rev. Phys. Chem., 37, 425 (1986).
5. R. D. Kelley and D. W. Goodman, Surf. Sci., 123, L743 (1982).
6. M. A. Vannice, J. Catal. 44, 152 (1976).
7. R. R. Wentrek, B. J. Wood, and H. Wise, J. Catal., 43, 363 (1976).
8. J. A. Rabo, A. P. Risch, and M. L. Poutsma, J. Catal., 53, 295 (1978).

9. M. Araki and V. Ponec, J. Catal., 44, 439 (1979).
10. D. W. Goodman, R. D. Kelley, T. E. Madey, and J. T. Yates, Jr., J. Catal. 64, 479 (1980)
11. D. W. Goodman and J. T. Yates, J. Catal., 82, 255 (1983).
12. D. W. Goodman and J. M. White, Surface Sci., 90, 201 (1979).
13. H. J. Krebs, H. P. Bonzel and G. Gafner, Surface Sci., 88, 269 (1979).
14. P. Biloen, J. N. Helle, and W. M. H. Sachtler, J. Catal., 58, 95 (1979).
15. (a) J. G. Ekerdt and A. T. Bell, J. Catal., 58, 179 (1979). (b) P. A. Dalla Betta and M. Shelef, J. Catal., 48, 111 (1977).
16. J. W. A. Sachtler, J. M. Kool and V. Ponec, J. Catal., 56, 84 (1979).

FIGURE CAPTIONS

Figure 1. An ultrahigh vacuum apparatus for studying single crystal catalysts before and after reaction at atmospheric pressure. (From refs. 3 and 4)

Figure 2. (a) A comparison of the rate of methane synthesis over single crystal nickel catalysts and supported Ni/Al_2O_3 catalysts at 120 Torr total reactant pressure. (From ref. 5) (b) Atomic configuration of a Ni(100) surface. (c) Atomic configuration of a Ni(111) surface.

Figure 3. A comparison of AES carbon signals on a Ni(100) crystal with those from single crystal graphite and nickel carbide. (a) Following 1000s heating at 700 K in 24 Torr CO. (b) Nickel carbide. (c) Following 1000s heating at 600 K in 24 Torr CO. (d) Single crystal graphite. (From refs. 3 and 4)

Figure 4. Methane production rate at 625 K over a Ni(100) catalyst as a function of surface carbon coverage at various reaction conditions. (From ref. 5)

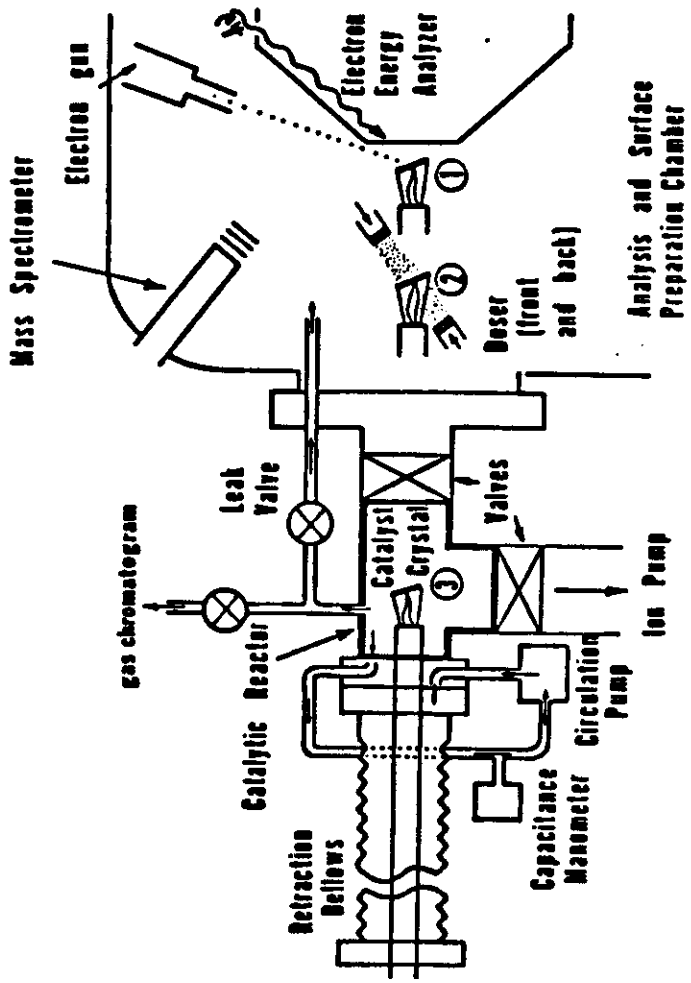

(1)

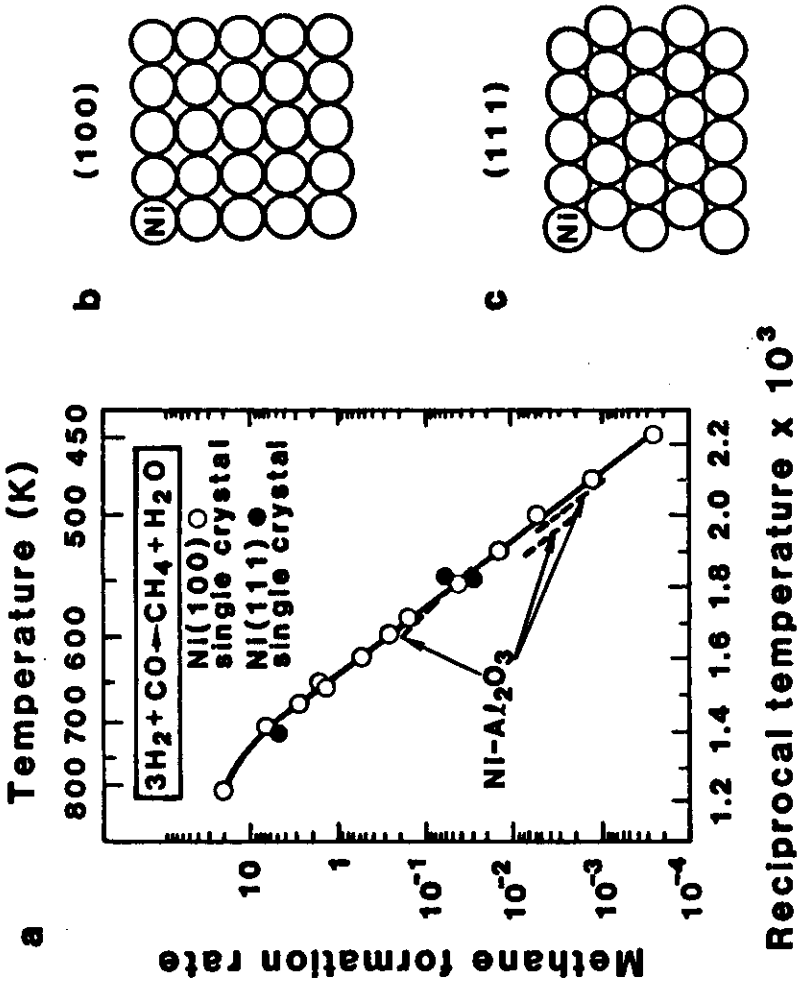
(100)
(111)
Ni
b
c
a
Temperature (K)
800 700 600 500 450
$3H_2+CO-CH_4+H_2O$
Ni(100) ○ single crystal
Ni(111) ● single crystal
Ni-Al_2O_3
10 1 10^{-1} 10^{-2} 10^{-3} 10^{-4}
Methane formation rate
1.2 1.4 1.6 1.8 2.0 2.2
Reciprocal temperature x 10^3

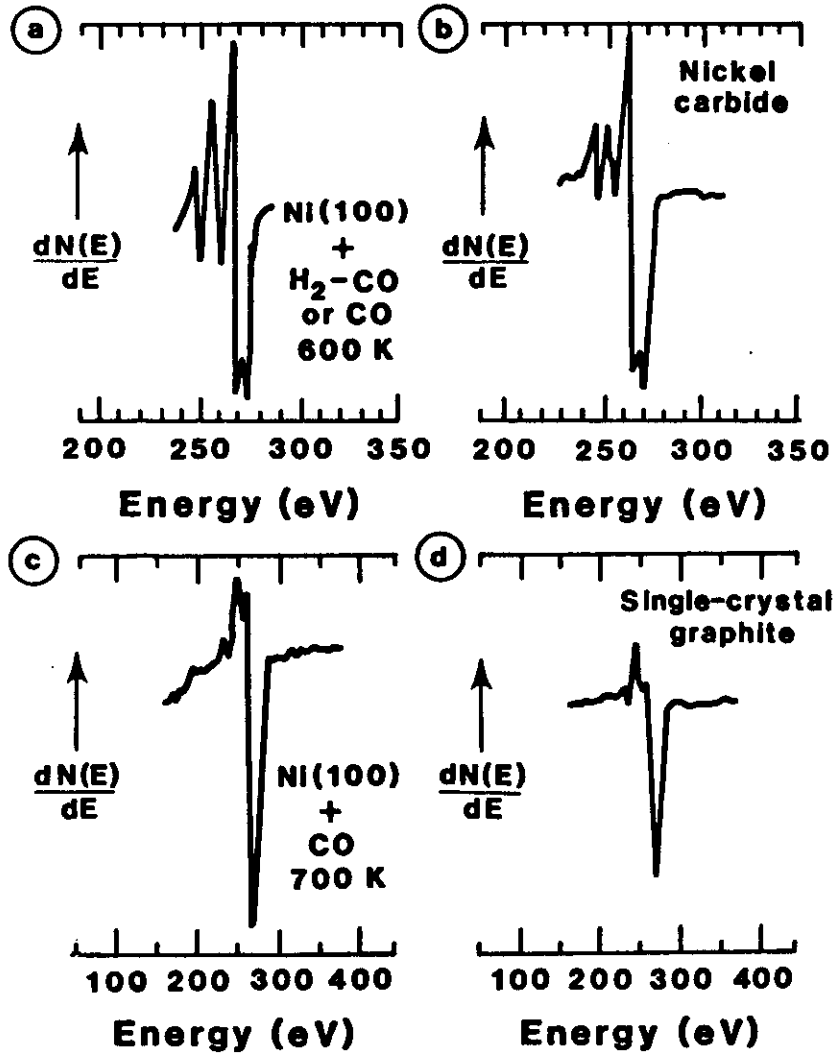
a
b
c
d
dN(E)/dE
Ni(100) + H_2-CO or CO 600 K
Nickel carbide
Ni(100) + CO 700 K
Single-crystal graphite
200 250 300 350
100 200 300 400
Energy (eV)

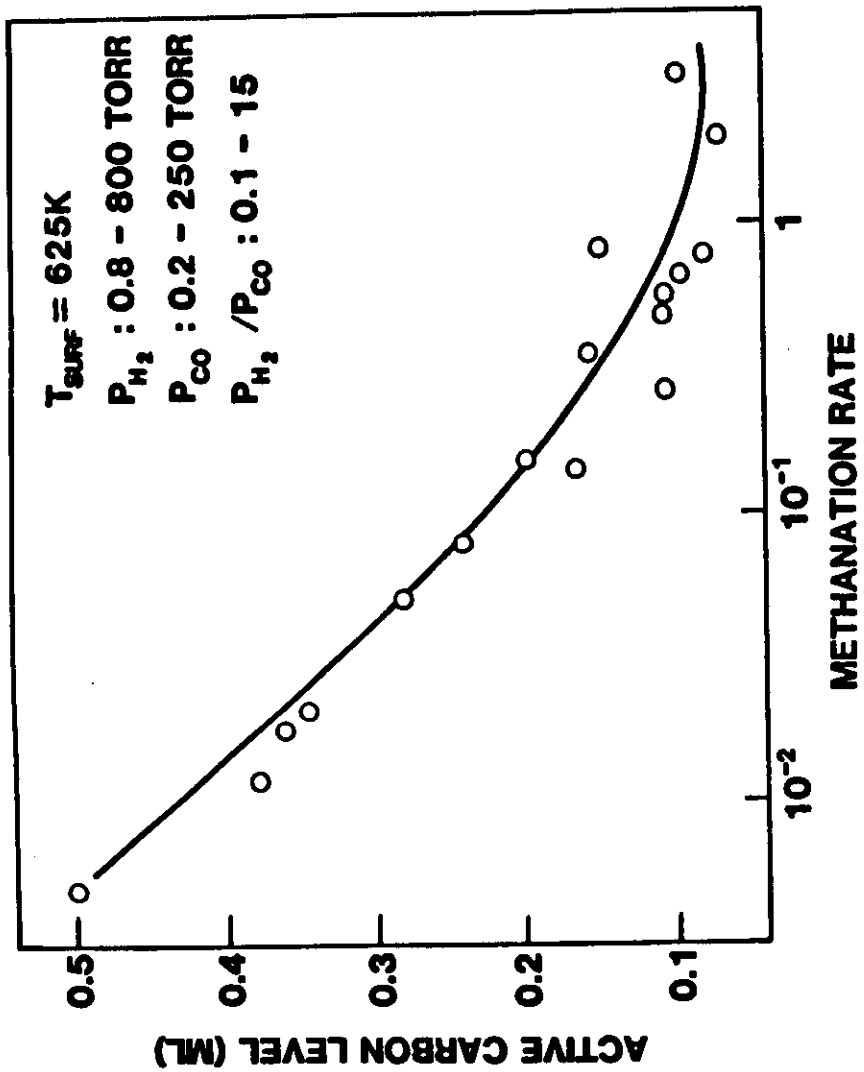

Correlations Between Surface Structure and Catalytic Properties: Structure-insensitive Reactions II. CO Oxidation

D. W. Goodman
Surface Science Division
Sandia National Laboratories
Albuquerque, NM 87185

ABSTRACT

The oxidation of CO over model Rh, Ru, Pt, Pd, and Ir single crystal catalysts has been studies in a high pressure reaction/UHV surface analysis apparatus. Steady-state activity as a function of temperature, CO and O_2 partial pressure dependence compare well with results obtained on high surface area catalysts. For all catalysts, in a stoichiometric O_2/CO mixture, the rates follow a simple Arrhenius rate law. In general, the reaction is positive first order in O_2 partial pressure and negative first order in CO partial pressure. These studies demonstrate the applicability and advantages of model single crystal studies, which combine UHV and surface analysis techniques with high pressure kinetic measurements, in the elucidation of reaction mechanisms over supported catalysts.

The oxidation of CO by O_2 over group VIII metal catalysts has been the subject of a large body of ultra-high vacuum surface science and high pressure catalysis work due to its importance in pollution control [1]. Currently, the removal of CO as CO_2 from automobile exhaust is accomplished by catalytic converters which employ a supported Pt, Pd, and Rh catalyst. The importance of CO oxidation has led to numerous recent studies of the kinetics of this reaction on supported metal catalysts [2-11] and transient kinetic studies on polycrystalline foils [12-21], which have sought to identify and quantify the parameters of the elementary mechanistic steps in CO oxidation.

The relative simplicity of CO oxidation makes this reaction an ideal model system of a heterogeneous catalytic reaction. Each of the mechanistic steps (adsorption and desorption of the reactants, surface reaction, and desorption of products) has been probed extensively with surface science techniques, as has the interaction between O_2 and CO [22-40]. These studies have provided essential information necessary for understanding the elementary processes which occur in CO oxidation.

Recent reviews by Ertl and Engel have summarized most of the chemisorption and low pressure catalytic findings [41,42]. In general, the reaction proceeds through a Langmuir-Hinshelwood mechanism involving adsorbed CO and O atoms. Under reaction conditions typical in most high pressure, supported catalyst studies, and most low pressure UHV studies, the surface is almost entirely covered by CO, and the reaction rate is determined by the rate of desorption of CO. As first determined by Langmuir for Pt wire catalysts [43], the observed activation energy is

close to the binding energy of adsorbed CO. Oxygen can only adsorb at sites where CO has desorbed, leading to first order dependence in oxygen pressure, negative first order in CO partial pressure, and zero order total pressure dependence. These features have allowed many of the reaction parameters determined in UHV to be applied directly to the kinetics at higher pressures [44].

Models based on chemisorption and kinetic parameters determined in surface science studies have been successful at predicting most of the observed high pressure behavior. Recently Oh et. al., [44] have modeled CO oxidation by O_2 or NO on Rh using mathematical models which correctly predict the absolute rates, activation energy, and partial pressure dependence. Similarly, studies by Schmidt and coworkers on CO + O_2 on Rh(111) [45] and CO + NO on polycrystalline Pt [46] have demonstrated the applicability of steady state measurements in UHV and relatively high (1 torr) pressures in determining reaction mechanisms and kinetic parameters.

Recently, the steady-state reaction kinetics of CO oxidation at high pressure over Ru [47], Rh [47-50], Pt, Pd, and Ir [51] single crystals has been studied in our laboratory. These studies have convincingly demonstrated the applicability and advantages of model single crystal studies, which combine UHV surface analysis techniques with high pressure kinetic measurements, in the elucidation of reaction mechanisms over supported catalysts.

These studies were carried out utilizing the specialized

apparatus described in references [52,53]. This device consists of two distinct regions, a surface analysis chamber and a microcatalytic reactor. The custom built reactor, contiguous to the surface analysis chamber, employs a retraction bellows that supports the metal single crystal and allows translation of the catalyst in vacuo from the reactor to the surface analysis region. Both regions are of ultrahigh vacuum construction, bakeable, and capable of ultimate pressures of less than 2 X 10^{-10} Torr. Auger spectroscopy (AES) is used to characterize the sample before and after reaction. A second chamber was equipped with Auger spectroscopy, low energy electron diffraction (LEED) and a mass spectrometer for temperature programmed desorption (TPD).

Figure 1 compares the CO oxidation rates measured over single crystals of Rh, Pt, Pd, Ir, and Ru with the analogous supported catalysts [25]. The turnover frequencies for the supported catalysts were obtained by normalizing the measured reaction rates to the total number of surface metal atoms. Notice that the turnover frequencies for the single crystal catalysts traverse several orders of magnitude over a temperature range of 450-600 K. Kinetic measurements over such a wide temperature range are not possible with supported catalysts due to heat and mass transfer limitations encountered at high temperatures. Thus, a direct comparison of the kinetic data between the two types of catalyst must necessarily be limited to a relatively small temperature range. Nevertheless, it is clear from Figure 1 that there is excellent agreement between the single crystal and supported catalysts in both the specific

reaction rates and apparent activation energies. This agreement indicates that CO oxidation is structure insensitive on nickel catalysts.

The Langmuir-Hinshelwood reaction between adsorbed CO and O atoms is well established as the dominant reaction mechanism for conditions where CO is the primary surface species [41,42]. This mechanism has been confirmed by numerous UHV studies of the co-adsorption of the reactants [13,22,23,26,27,29,31,32,34, 36,40], transient kinetic studies [58,14,16,17,18,19,21,24], and steady state kinetics [15,30,33,37,38,39]. The reaction steps may be written as:

$$CO(g) \text{ <---> } CO(a) \qquad (1)$$

$$O_2(g) \text{ ---> } 2O(a) \qquad (2)$$

$$CO(a) + O(a) \text{ ---> } CO_2(g) \qquad (3)$$

where recombinative desorption of O_{ads} (the reverse of reaction 2) and dissociative chemisorption of CO_2 (the reverse of reaction 3) are neglected. From the above, an approximate rate expression, originally proposed by Langmuir for Pt [43], can be formulated as:

$$dCO_2/dt = k \exp(-E_{des,CO}/RT) P_{O2}/P_{CO} \qquad (4)$$

Thus, the reaction rate is independent of total pressure, first order in O_2 pressure, and negative first order in CO pressure. One obtains equation 4 by assuming that the dominant surface species is CO [44]. The rate is then governed by the desorption of CO and the pressure dependence simply reflects the competition for adsorption sites between O_2 and CO. The measured kinetics on Rh, Pd, Ir, and Pt at high temperatures, are consistent with this model in that the predicted pressure

dependencies are observed [51]. In addition, the correlation in activation energies between supported and single crystal data, and among different single crystal planes, reflects the fact that the binding energy of CO does not vary greatly among these metal catalyst surfaces.

Figure 2 shows the dependence of the rate of CO oxidation over the single crystal catalysts on the partial pressure of CO. At conditions of relatively high partial pressures of CO, the reaction rate is observed to decrease linearly with increasing CO partial pressure reflecting the domination of reactant surface coverage by CO. For these reaction conditions on Rh, this behavior has been accurately modeled [44] using individual elementary reaction steps established from surface science studies of the interactions of CO and O_2 with Rh.

The rate of CO oxidation as a function of oxygen partial pressure at similar catalyst temperatures as the measurements in figure 2 and at a fixed CO partial pressure are shown in Figure 3. The rates, in general, exhibit a first-order dependence on the partial pressure of O_2 at P_{O2} < 100 Torr. As the oxygen partial pressure is increased further, however, on Rh, Pd and Ir the CO oxidation rate is observed to roll over with a maximum activity occurring at approximately O_2/CO = 30. For larger O_2/CO ratios, the reaction becomes positive order in CO and negative order in O_2 pressure on these surfaces. For Pt, CO oxidation is first order in oxygen pressures over the entire pressure range studied, while on Ru, the reaction is positive order in O_2 pressure at low pressures, and zero order for O_2/CO ratios

greater than 1/4.

The condition of the catalyst surface, and the origin of the partial pressure dependence at high O_2/CO ratios is not as clear as is the case for low O_2/CO ratios. On Rh(100) and (111) [48] and Ru(0001) [47], changes in the rates and partial pressure dependencies have been directly correlated with the formation of a strongly bound oxygen species. On Ru, the oxide is substantially more active than the clean surface and the reaction order in oxygen pressure is close to three at low O_2 pressures, reflecting the gradual formation of the oxide layer as the O_2 pressure is increased. Once the oxide is fully formed, the reaction rate becomes zero order in oxygen pressure. On Rh(111) and (100) single crystals increases in the O_2/CO ratios result in an eventual decrease in rates, and a change from positive order in oxygen to negative order. This change has been correlated directly with the formation of an oxide-like species, characterized by AES and TPD subsequent to reaction [48], which is less active than the clean surfaces. Pd(110), Ir(111), and Ir(110) exhibit partial pressure dependence and high oxygen pressure deactivation behavior which are very similar to Rh. In the case of Rh, the formation of a near surface oxide (probably Rh_2O_3 [50] which is catalytically inactive) is responsible for the deactivation. The similar behavior on Pd and Ir suggests that oxide formation is also responsible for the deactivation on these metals. In contrast to Rh, however, the oxide species cannot be isolated on Pd and Ir. Instead, the strongly bound oxygen species reacts with CO and is detected as CO_2, which desorbs at high temperatures in post-reaction TPD. Thus, the

oxide formed on Rh is resistant to reduction by CO in the post-reaction cool-down and transfer, while oxide reduction by CO is quite facile on Pd and Ir.

The metal surfaces are always covered with a monolayer of CO upon evacuation of the reactor and transfer to the UHV system. On both Pd and Ir the CO, which desorbs as CO_2 when reacted with the oxide species, desorbs at a much higher temperature than CO from the clean surface. This result implies that the oxide species forms an inactive complex with CO upon adsorption of CO under reaction conditions. While the presence of the oxide species reduces the overall rate of reaction, the activation energy is unchanged, suggesting that oxygen serves as a simple site blocker on the surface.

The differences between Pt, Pd, Ir, Ru and Rh may be explained by the ease of oxidation of these metals. The more easily oxidized Rh (and Ru) surfaces form oxides which are bound strongly enough to resist reaction when CO is flashed off the crystal prior to post-reaction AES analysis. Pd and Ir, which are less easily oxidized than Rh, form a less strongly bound oxide, possibly in a thinner layer, which is easily reduced. In a study by Savchenko and coworkers [54], it was shown that a reconstructive type of oxygen adsorption (i. e. the formation of an oxide) would only occur for metals with a heat of adsorption of oxygen above 220 kJ/mol. Pt falls well below this limit; Pd, Rh, and Ir are close to the borderline between types of oxides; while Ru falls well into the oxide range. This evaluation corresponds well with the observed oxidation behavior of these

metals during CO oxidation.

For Pt(100) the lack of any turnover in the oxygen partial pressure behavior (figure 3) indicates that under our conditions no strongly bound, deactivating oxygen species is formed. In light of the trend from Ru to Rh to Pd and Ir, this is not surprising. In order to form an oxide species on Pt, much higher O_2 pressures and/or higher temperatures would be required.

It is interesting to compare our results on single crystal surfaces with those of Turner and coworkers [55] for Pt, Pd, and Ir. In this study wires of Pt formed less than one layer of "oxide" under CO oxidation conditions. Considering that the Pt wires were known to have substantial Si impurities, which form subsurface oxides [56-58], it is not surprising that some oxide was formed. The absence of impurities on the rigorously cleaned, Pt single crystal surface used in this study precluded the formation of any oxides during CO oxidation.

ACKNOWLEDGEMENT

We acknowledge with pleasure the partial support of this work by the Department of Energy, Office of Basic Energy Sciences, Division of Chemical Sciences.

REFERENCES

1. J. T. Kummer, J. Phys. Chem., 90, 4747 (1986).
2. N. W. Cant, P. C. Hicks, and B. S. Lennon, J. Catal., 54, 372 (1978).
3. J. T. Kiss and R. D. Gonzalez, J. Phys. Chem., 88, 892 (1984).
4. J. T. Kiss and R. D. Gonzalez, J. Phys. Chem., 88, 898 (1984).
5. S. E. Oh, J. E. Carpenter, J. Catal., 80, 472 (1983).
6. Y. Y. Yu, J. Catal., 87, 152 (1984).
7. H. Okamoto, G. Kawamura, and T. Kudo, J. Catal., 87, 1 (1984).
8. N. W. Cant and D. E. Angove, J. Catal., 97, 36 (1986).
9. R. C. Shishu, L. S. Kowalczyk, Platinum Metals Rev., 18, 58 (1984).
10. S. E. Voltz, C. R. Morgan, D. Liederman, and S. M. Jacob, Ind. Eng. Chem. Prod. Res. Dev., 12, 294 (1973).
11. D. M. Nicholas and Y. T. Shah, Ind. Eng. Prod. Res. Dev., 15, 35 (1976).
12. J. L. Taylor, D. E. Ibbotson, and W. H. Weinberg, Surf. Sci., 90, 37 (1979).
13. T. Matsushima, J. Phys. Chem., 88, 202 (1984).
14. T. Matsushima and J. M. White, J. Catal., 39, 265 (1975).
15. M. Kawai, T. Onishi, and K. Tamaru, Appl. Surf. Sci., 8, 361 (1981).
16. T. Matsushima, C. J. Mussett, and J. M. White, J. Catal. 41, 397 (1976).
17. T. Matsushima, J. Catal., 55, 337 (1978).
18. G. K. Hori, and L. D. Schmidt, J. Catal., 38, 335 (1975).
19. J. M. White and A. Golchet, J. Chem. Phys., 66, 5744 (1977).
20. E. McCarthy, J. Zahradnik, G. C. Kuczynski, and J. J. Carberry, J. Catal., 39, 29 (1975).
21. T. Matsushima, Surf. Sci., 79, 63 (1979).

22. D. I. Hagen, B. E. Nieuwenhuys, G. Rovida, and G. A. Somorjai, Surf. Sci., 57, 632 (1976.
23. J. Kuppers, and A. Plagge, J. Vac. Sci. Technol., 13, 259 (1986).
25. V. P. Zhdanov, Surf. Sci., 137, 515 (1984).
26. P. A. Zhdan, G. D. Boreskov, A. I. Boronin, A. P. Schepelin, S. P. Withrow, and W. H. Weinberg, Appl. Surf. Sci., 3, 145 (1979).
27. P. A. Zhdan, G. K. Boreskov, W. F. Egelhoff, Jr., W. H. Weinberg, Surf. Sci., 61, 377 (1976).
28. V. Matolin and E. Gillet, Surf. Sci., 166, L115 (1986).
29. E. M. Stuve, R. J. Madix, and C. R. Brundle, Surf. Sci., 146, 155 (1984).
30. T. Engel and G. Ertl, J. Phys. Chem., 69, 1267 (1978).
31. H. Conrad, G. Ertl, and J. Kuppers, Surf. Sci., 76, 323 (1978).
32. D. A. Mantell, S. B. Ryali, and G. L. Haller, Chem. Phys. Lett., 102, 37 (1983).
33. V. Matolin, E. Gillet, and M. Gillet, Surf. Sci., 162, 354 (1985).
34. T. Engel, J. Chem. Phys., 69, 373 (1978).
35. R. J. Behm, P. A. Thiel, P. R. Norton, and P. E. Binder, Surf. Sci., 147, 143 (1984).
36. S. Akhter and J. M. White, Surf. Sci., 171, 527 (1986).
37. T. Matsushima and H. Asada, J. Chem. Phys., 85, 1658 (1986).
38. R. L Palmer and J. N. Smith, Jr., J. Chem. Phys., 60, 1453 (1974).
39. C. T. Campbell, G. Ertl, H. Kuipers, and J. Segner, J. Chem. Phys., 73, 5862 (1980).
40. J. L. Gland and E. B. Kollin, J. Chem. Phys., 78, 963 (1983).
41. T. Engel and G. Ertl, Adv. Catal., 28, 1 (1979).
42. T. Engel and G. Ertl in "The Chemical Physics of Solid Surfaces and Heterogeneous Catalysts, Vol 4," D. A. King and D. P. Woodruff, eds. Elsevier, Holland, 1982.

43. I. Langmuir, Trans. Farad. Soc., 17, 621 (1921-22).

44. S. H. Oh, G. B. Fisher, J. E. Carpenter, and D. W. Goodman, J. Catal., 100, 360 (1986).

45. S. B. Schwartz, L. D. Schmidt, and G. B. Fisher, J. Phys. Chem., 90, 6194 (1986).

46. R. L. Klein, S. Schwartz, and L. D. Schmidt, J. Phys. Chem., 89, 4908 (1985).

47. C. H. F. Peden and D. W. Goodman, J. Phys. Chem., 90, 1360 (1986).

48. C. H. F. Peden, D. W. Goodman, D. S. Blair, P. J. Berlowitz, G. B. Fisher, and S. H. Oh, submitted to J. Phys. Chem.

49. D. W. Goodman and C. H. F. Peden, J. Phys. Chem., 90, 4839 (1986).

50. G. L. Kellogg, J. Catal., 92, 167 (1985).

51. P. J. Berlowitz, C. H. F. Peden and D. W. Goodman, J. Phys. Chem., submitted.

52. D. W. Goodman, R. D. Kelley, T. E. Madey, and J. T. Yates, Jr., J. Catal. 64, 479 (1980).

53. D. W. Goodman, Ann. Rev. Phys. Chem., 37 (1986) 425; D. W. Goodman, Accts. Chem. Res., 17, 194 (1984); D. W. Goodman, J. Vac. Sci. Tech., 20, 522 (1982).

54. V. I. Savchenko, G. K. Boreskov, A. V. Kalinkin, and A. N. Salanov, Kinetics and Catalysis, 24, 983 (1984).

55. B. C. Sales, J. E. Turner, and M. B. Maple, Surf. Sci., 112, 272 (1981).

56. H. Niehus and G. Comsa, Surf. Sci., 93, L147 (1980).

57. H. Niehus and G. Comsa, Surf. Sci., 102, L14 (1981).

58. H. P. Bonzel, A. M. Franken, and G. Pirug, Surf. Sci., 104, 625 (1981).

FIGURE CAPTIONS

Figure 1. Specific rates of CO oxidation (turnover frequencies) as a function of inverse temperature for single crystal and supported Ru, Pt, Ir, and Pd catalysts. (From refs. 47-51)

Figure 2. The CO partial pressure dependence at constant oxygen pressure for single crystal Rh, Ru, Pt, Ir, and Pd catalysts. (From refs. 49-51)

Figure 3. The O_2 partial pressure dependence at constant CO pressure for single crystal Rh, Ru, Pt, Ir, and Pd catalysts. (From refs. 49-51)

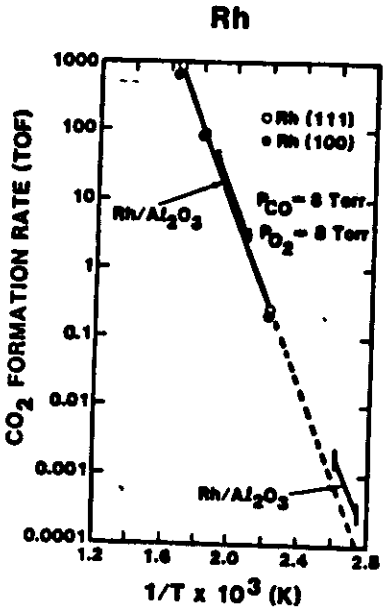
Rh
CO2 FORMATION RATE (TOF)
1000
100
10
1
0.1
0.01
0.001
0.0001
Rh (111)
Rh (100)
Rh/Al2O3
PCO = 8 Torr
PO2 = 8 Torr
Rh/Al2O3
1.2
1.6
2.0
2.4
2.8
1/T x 10^3 (K)

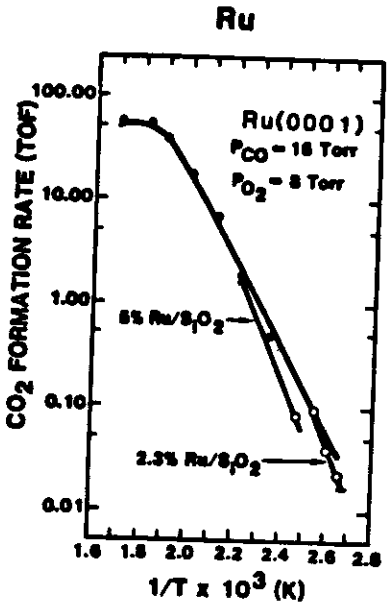
Ru
CO2 FORMATION RATE (TOF)
100.00
10.00
1.00
0.10
0.01
Ru(0001)
PCO = 16 Torr
PO2 = 8 Torr
5% Ru/SiO2
2.3% Ru/SiO2
1.6
1.8
2.0
2.2
2.4
2.6
2.8
1/T x 10^3 (K)

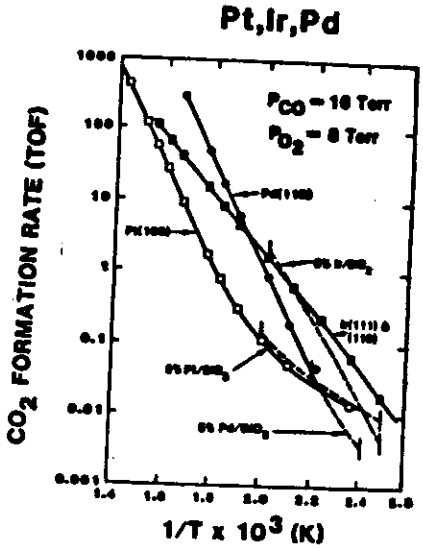
Pt,Ir,Pd
CO2 FORMATION RATE (TOF)
PCO = 16 Torr
PO2 = 8 Torr
1/T x 10^3 (K)

(1)

28

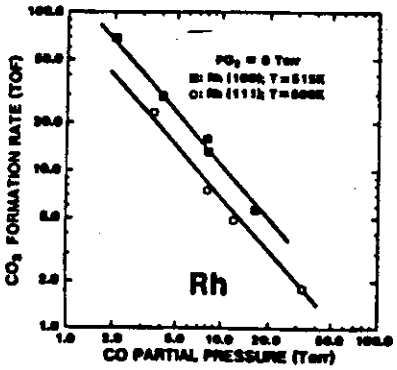
CO2 FORMATION RATE (TOF)
Rh
CO PARTIAL PRESSURE (Torr)

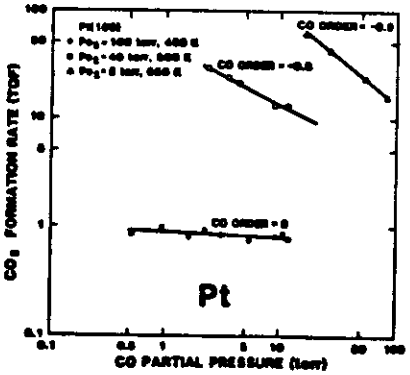
CO2 FORMATION RATE (TOF)
Pt
CO PARTIAL PRESSURE (torr)

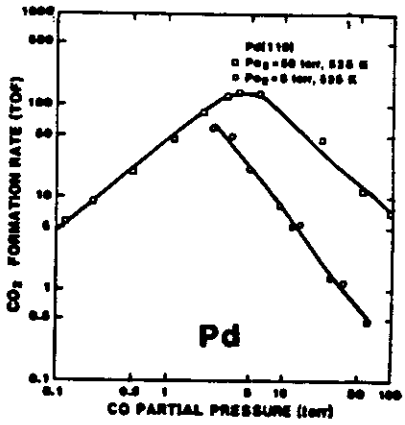
CO2 FORMATION RATE (TOF)
Pd
CO PARTIAL PRESSURE (torr)

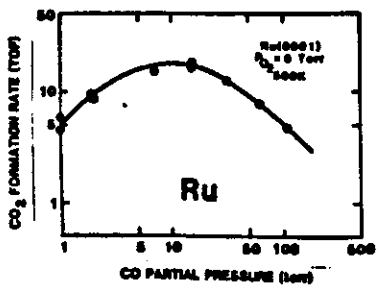
CO2 FORMATION RATE (TOF)
Ru
CO PARTIAL PRESSURE (torr)

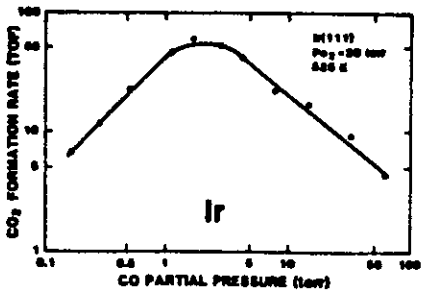
CO2 FORMATION RATE (TOF)
Ir
CO PARTIAL PRESSURE (torr)

(2)

29

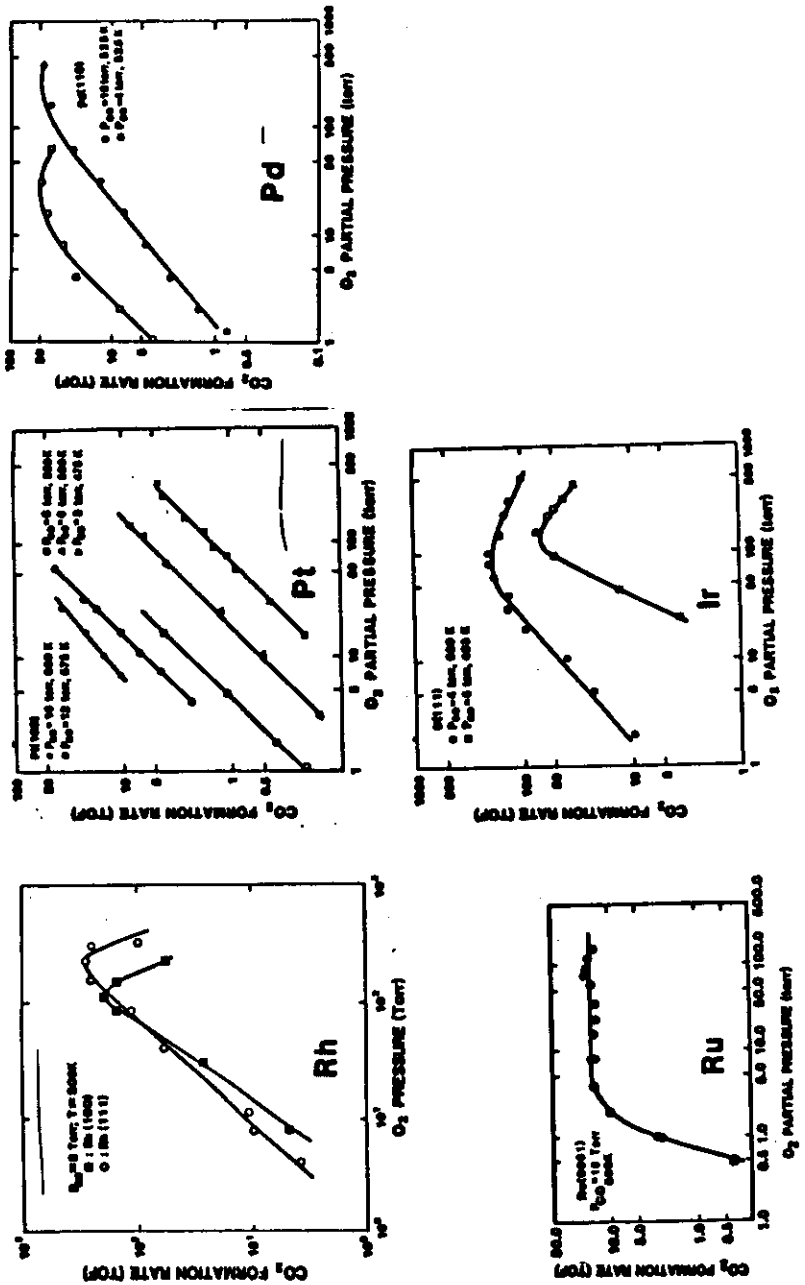

Correlations Between Surface Structure and Catalytic Properties: Structure-sensitive Reactions

D. W. Goodman
Surface Science Division
Sandia National Laboratories
Albuquerque, NM 87185

ABSTRACT

The dissociative adsorption and reaction of small alkanes has been investigated on single crystalline surfaces of Ni, Ir, and Rh. These studies have utilized a coupled high pressure reactor-ultrahigh vacuum analysis chamber, which permits both the measurement of the specific rates of reaction and in situ pre- and post-reaction surface characterization. Both the apparent reaction kinetics and the dependence of the rates of reaction on the reactant partial pressures have been examined in detail.

The selectivity for hydrogenolysis on the "rough" or more open surfaces of Ni, Ir and Rh surfaces [Ni(100), Ir(110)-(1x2) and Rh(110)] correlates well with analogous results for relatively small particles of Ni, Ir and Rh in supported catalysts. The results for the "smooth" Ni, Ir and Rh surfaces [Ni(111), Ir(111) and Rh(111)], on the other hand, correlate well with the analogous results for relatively large supported particles of Ni, Ir and Rh.

Altogether these results are suggestive regarding the nature of the active sites on these catalytic surfaces for alkane reaction and rearrangement.

(3)

The activation of alkanes on transition metal surfaces is an important step in many catalytic reactions. Hydrogenolysis, steam reforming and isomerization of alkanes all involve alkane dissociation. Thus, much interest exists in the mechanistic and kinetic aspects of alkane dissociation.

Relative to most other classes of organic molecules, alkanes are very unreactive at transition metal surfaces. While alkane dissociation is easily observable at high pressures on transition metal surfaces [1-3] the activation of alkanes in ultra-high vacuum, where the analytical tools of surface science can provide detailed mechanistic and structural information, is quite difficult. In vacuum, low surface temperatures are required to stabilize molecular adsorption of alkanes [4-8]. Subsequent heating of the surfaces generally results in molecular desorption of the adsorbed alkanes without any detectable decomposition or reaction [4,9-11]. Two exceptions to this behavior are the Pt(110)-(1x2) [8] and Ir(110)-(1x2) [5,7] surfaces on which alkanes undergo dissociation at 200 K and 130 K, respectively. The high reactivity of these two surfaces for alkane decomposition has been related to the presence of low coordination metal atoms formed as a result of the (1x2) reconstruction [8] The absence of dissociation on other single crystal transition metal surfaces indicates that the barriers to dissociation are generally too large for dissociation to compete effectively with desorption during TPD.

In order to overcome the barrier to dissociation in ultra-high vacuum, several workers have used high energy molecular beams [12-19]. By far the most attention has been devoted to

methane dissociation, although studies of the dissociation of higher alkanes on Ni(100) [14] and Ir(110)-(1x2) [13] have also been reported. While the use of molecular beams clearly enables one to observe alkane dissociation in vacuum, molecular beam techniques generally sample only the behavior of high energy molecules, providing relatively little information regarding the behavior of the low energy molecules which dominate the flux at surfaces at high pressures. Thus, it is not clear, a priori, that the dissociation behavior observed by molecular beam techniques accurately reflects the processes which occur at high pressures.

These studies were carried out utilizing the specialized apparatus described in references [20,21]. This device consists of two distinct regions, a surface analysis chamber and a microcatalytic reactor. The custom built reactor, contiguous to the surface analysis chamber, employs a retraction bellows that supports the metal single crystal and allows translation of the catalyst in vacuo from the reactor to the surface analysis region. Both regions are of ultrahigh vacuum construction, bakeable, and capable of ultimate pressures of less than 2×10^{-10} Torr. Auger spectroscopy (AES) is used to characterize the sample before and after reaction. A second chamber was equipped with Auger spectroscopy, low energy electron diffraction (LEED) and a mass spectrometer for temperature programmed desorption (TPD).

In order to determine if the results of the molecular beam studies can indeed be used to predict dissociation kinetics at

high pressures, Beebe, et al. [22], measured dissociative sticking coefficients of methane at 1.0 Torr on the three low index surfaces of nickel, and compared their results to molecular beam studies by Hamza and Madix [14] on Ni(100) and Lee, et al. [16,17] on Ni(111). It was found that the activity of the nickel surfaces for methane dissociation increased in the order Ni(111) < Ni(100) < Ni(110), with activation energies of 12.6, 6.4, and 13.3 kcal/mole, respectively. The absolute magnitudes of the sticking probabilities were quite small, falling in the range of 10^{-7} to 10^{-9} for all three surfaces. In addition, on Ni(100) and Ni(110), the effect of deuterium substitution on methane dissociation was found to be consistent with a mechanism involving quantum tunneling of a proton as the rate limiting step [22]. This finding is consistent with studies of methane activation on other transition metal surfaces [18,19,23], which all suggest a tunneling mechanism. The deuterium isotope effect was not measured for Ni(111).

As shown in figure 1, good agreement was obtained between the high pressure data [22] and the molecular beam data for Ni(111) [16,17]. The dissociative sticking probabilities measured at 1.0 Torr were only a factor of four greater than predicted by the beam experiments, well within the combined uncertainty of the two studies. In contrast, very poor agreement was obtained between the high pressure data [22] and the molecular beam data [14] on the Ni(100) surface. As shown in figure 8, sticking probabilities measured at 1.0 Torr were a factor of 100 to 200 lower than the values predicted from the molecular beam data. This disagreement is now believed to be due

to differences in vibrational excitation of the methane molecules between the two studies [24]. In order to achieve the high translational energies necessary for methane activation, nozzle temperatures as high as 1000 K were used in the molecular beam study [24], resulting in significant vibrational excitation of the incident methane molecules. At the temperatures used in the high pressure study, relatively little vibrational excitation occurs. For both the W(110) [18,19] and Ni(111) [16,17] surfaces, vibrational excitation has been shown to be as effective as translational energy in promoting methane dissociation. Assuming that vibrational excitation also promotes dissociation on Ni(100), then the presence of large amounts of vibrational energy in the beam experiments may have resulted in an overestimation of the dissociative sticking probabilities of methane at high pressures. In fact, Kay [24] has shown that by correcting the molecular beam data for the effects of vibrational excitation, good agreement can be obtained between the molecular beam study and the high pressure study.

It should be noted that vibrational excitation of the incident methane molecules was also present in the molecular beam study of methane on Ni(111) [17]. In that case, however, the contributions of vibrational energy to the sticking coefficients were carefully subtracted out of the data, so that the reported sticking probabilities reflected only the effects of translational energy. Thus, the differences in vibrational excitation between the beam study [17] and the high pressure study [22] were negligible, and good agreement was obtained

between the two studies.

Sault and Goodman [26] have recently extended the study of Beebe, et al. [22] to the higher alkanes. As was the case for methane, the object of this study was to compare sticking probabilities measured at high ambient pressures with the results of a molecular beam study by Hamza and Madix [14]. The work was confined to the Ni(100) surface as this is the only plane of nickel on which dissociation of higher alkanes has been studied using molecular beam techniques.

Using alkane-helium mixtures with alkane partial pressures from 0.001 to 0.1 Torr and total pressures of 1.0 torr to ensure thermal equilibrium between the surface and the ambient gas, Sault and Goodman [26] found that the sticking probabilities for alkanes on Ni(100) increased in the order methane < ethane < propane < n-butane, with activation energies of 6.4, 9.5, 3.8 and 3.1 kcal/mole, respectively. In contrast to methane, no measurable deuterium kinetic isotope effect was found for ethane dissociation. This result indicates that proton tunneling is not the dominant mechanism for dissociation of the higher alkanes. The possibility that proton tunneling is a minor pathway to ethane dissociation cannot be ruled out, however.

Comparison of the dissociative sticking probabilities measured at high pressures with the predictions of the molecular beam study are shown in Figure 2. For all of the higher alkanes, the agreement is very poor. The absolute values of the sticking coefficients measured at high pressure are all greater than predicted by the molecular beam data. In addition, the activation energies for dissociation and the effect of increasing

carbon chain length are also in disagreement. The discrepancies are believed to be due to the behavior of very low energy molecules, which dominate the flux at the surface at high pressures [26], but are very difficult to examine using molecular beam techniques. Hamza and Madix [14] reported a linear increase in the dissociation probabilities of ethane, propane and n-butane with normal kinetic energy for energies above a threshold of 50 kJ/mole. The slope of this linear increase decreased in the order ethane > propane > n-butane. Below the threshold, no dissociation could be detected, but the smallest sticking probability which could be measured by Hamza and Madix was on the order of 10^{-4} [25]. From Figure 2 it can be seen that all of the sticking probabilities measured at high pressures are well below 10^{-4}. Thus, if alkane molecules with energies below the threshold dissociate with nonzero probabilities which are less than 10^{-4}, then the discrepancies in the magnitude of the sticking probabilities and activation energies for dissociation shown in Figure 2 can be accounted for [26].

To account for the fact that the dissociation probabilities measured in the beam experiments increased in the order n-butane < propane < ethane < methane, while the opposite trend was observed at high pressures, it must be assumed that different dissociation mechanisms operate for low and high energy molecules. At the high energies at which Hamza and Madix [14] were able to observe dissociation, a direct mechanism for dissociation occurs. Hamza and Madix [14] postulate that for the direct mechanism, dissipative transfer of translational energy

out of the reaction channel into surface phonons and internal modes of the alkanes can explain the observed variation of the sticking probability with carbon chain length. As the chain length increases, the amount of dissipative transfer also increases, thereby decreasing the fraction of the incident translational energy which is transfered into the reaction channel and resulting in the observed decrease in sticking probability with increasing carbon chain length. The low energy molecules which dominate the dissociation kinetics at high pressures are believed to dissociate via a trapped molecular precursor [26]. Since both the trapping probability and the surface lifetime of the trapped alkanes increases in the order ethane < propane < n-butane, the sticking probabilities also increase in this order at high pressures.

Based on the studies of alkanes dissociation at high pressures, two conclusions were reached regarding the applicability of molecular beam studies for predicting high pressure behavior [26]. First, the effects of vibrational excitation must be accounted for in order to make accurate predictions. Only in cases where the vibrational excitation produced during formation of the molecular beam is similar to that in the high pressure process being modeled will good agreement be obtained between high pressure and molecular beam studies. Second, the behavior of low energy molecules is critically important in determining the high pressure behavior, since the flux of molecules at a surface is dominated by low energy molecules [26]. Only in cases where the behavior of low energy molecules is accurately measured will molecular beam

techniques be able to reliably predict high pressure behavior.

Finally, it should be pointed out that the rates of alkane dissociation on the clean nickel surfaces are generally somewhat greater than the rates of hydrogenolysis and steam reforming of the alkanes [22,26]. This result is expected since both steam reforming and hydrogenolysis take place on partially carbon covered surfaces and carbon is known to inhibit alkane dissociation. Furthermore, it is not entirely clear that the dissociation step is rate limiting for either steam reforming or hydrogenolysis. Thus, the rates of alkane dissociation measured on the clean surfaces represent a theoretical upper limit for the rates of steam reforming and hydrogenolysis on unpromoted nickel surfaces.

The activity of metal catalysts toward alkane hydrogenolysis generally depend markedly on the metal particle size and upon the nature of the metal [27,28]. These reactions have therefore been described as structure sensitive. Although there is a consensus in the literature regarding the relationship of particle size to activity, no such consensus exists in detailing the origins of the effect. Work by Martin [27] suggests that different activities of different crystal planes toward a given reaction could be responsible for the observed rate attenuation with increasing particle size. For example, if (111) orientations become dominant as the metal particles become larger and if these crystal planes exhibited a lower activity toward hydrogenolysis, then the activity of the catalyst would fall with particle growth. Martin further speculated that the lower activity of the

(111) facet relative to other facets could be intrinsic or could arise from preferential poisoning of the (111) crystal plane by reactants or products. These studies emphasized the need for kinetic measurements over single metal catalysts. Such studies have been carried out for the hydrogenolysis of ethane [30], n-butane [31], and cyclopropane Ni111 and Ni(100) [32]. These results confirm that Ni(111) is indeed significantly less active toward hydrogenolysis than Ni(100). This reduced activity has been shown to be intrinsic and not due to selective poisoning of the (111) surface by carbon.

Fig. 3 shows the specific reaction rate for methane formation from ethane over a Ni(100) catalyst. At a given temperature the rate of methane production over an initially clean crystal was constant with no apparent induction period. The carbon level during reaction remained constant at a submonolayer coverage. The methane turnover frequency during a fixed time (typically 1000s) was determined using the Ni(100) atom density of 1.62×10^{15} atoms/cm^2.

Figure 3 shows the kinetic data for ethane hydrogenolysis over a Ni(111) catalyst. As observed for the (100) catalyst, the carbon level during reaction remained constant at submonolayer coverages. The specific rate was determined using the Ni(111) atom density of 1.88×10^{15} atoms/cm^2. It is evident that the activity of the (111) surface toward ethane hydrogenolysis is considerably less than that observed for the (100) surface as suggested by Martin [29]. The kinetic results for the Ni(111) catalyst agree favorably with the data of Martin [29] for Ni/SiO_2 catalysts reduced at high temperature with a resulting larger

particle size. Such severely sintered catalysts are expected to contain metal crystallites exposing predominantly (111) faces [33].

The origin of the lower activity associated with the (111) surface compared with the (100) is not presently understood. We can speculate that electronic differences, which most certainly exist, are responsible. An additional contribution could be the spatial distribution of the high coordination bonding sites [30], those on the (111) surface being more favorable for stabilization of C_2 fragments. The result of this stabilization is that the (111) surface is less effective in cleaving carbon-carbon bonds, an obvious crucial step in hydrogenolysis.

Both the Ir(110)-(1x2) [5-7] and Pt(110)-(1x2) [8] surfaces are unique in that they are the only known surfaces on which adsorbed alkanes dissociate during TPD in ultra-high vacuum. This behavior is clearly related more to the structure of these reconstructed surfaces than to the specific nature of the metal as dissociation does not occur on the (111) surfaces of either Pt [4] or Ir [6]. In order to more fully understand the relationship between surface structure and catalytic activity and selectivity, Engstrom, et al. [34-36] studied the hydrogenolysis of a number of alkanes on the (110)-(1x2) and (111) surfaces of iridium. These reactions were conducted at total pressures on the order of 100 Torr, hydrogen:hydrocarbon ratios of 100:1 and temperatures in the range 425-625 K [34-36]. Total conversions were kept below 1% in order to avoid further hydrogenolysis of reaction products. Reaction orders in both the hydrocarbons and

hydrogen were also investigated.

Before reviewing reactions of the individual hydrocarbons, some overall trends will be discussed. In general, post-reaction surface analysis by AES showed the presence of submonolayer coverages of carbon, with a fractional coverage fairly independent of reaction conditions for a given alkane. The amount of carbon left on the surface increased approximately linearly with the size of the parent hydrocarbon molecule. This carbon residue is not believed to be an important intermediate in the hydrogenolysis reactions [35,36], however, and will not be discussed further. For all of the linear hydrocarbons and both the Ir(111) and Ir(110)-(1x2) surfaces, Arrhenius plots of product formation rate vs. temperature were linear at low temperatures, but showed large deviations from linearity at higher temperature. Simultaneous with the deviations from linearity, the selectivity of the reaction moved toward more complete hydrogenolysis, i.e., the relative production of methane increased at the expense of higher alkanes. The high temperature deviations are related to a decrease in the steady-state coverage of hydrogen as the temperature approaches the desorption temperature of hydrogen [35,36]. Because the binding energy of hydrogen on Ir(110)-(1x2) is greater than on Ir(111) [37,38], the deviations from linearity occur at a higher temperature on Ir(110)-(1x2) than on Ir(111) [88,egw1].

Different kinetic parameters were observed for ethane hydrogenolysis on the two surfaces [35]. The activation energies and preexponential factors for hydrogenolysis are 35 kcal/mole and $1x10^{13}$ s^{-1} on Ir(111) and 49 kcal/mole and $6x10^{18}$ s^{-1} on

Ir(110)-(1x2). The differences in these parameters indicate that a different mechanism operates on the two surfaces. Based on kinetic modeling, it is believed that hydrogenolysis proceeds through a C_2H_4 intermediate on Ir(111) and a C_2H_2 intermediate on Ir(110)-(1x2). The C_2H_2 species can be stabilized on the Ir(110)-(1x2) surface by adsorption in the trough sites, which allows greater coordination of the C_2H_2 species to the surface than is possible on the flat Ir(111) surface. Because of the differences in activation energy, the relative rates of hydrogenolysis on the two surfaces crossover near 550 K, with Ir(111) being more active below 550 K and Ir(110)-(1x2) being more active above 550 K. This crossover explains why no structure sensitivity was observed in a study of ethane hydrogenolysis on supported iridium catalysts [39] at temperatures of 525-550 K.

At low temperatures on both surfaces, propane hydrogenolysis involves cleavage of a single C-C bond to produce equal amounts of methane and ethane [35]. At high temperatures the relative rate of methane production increases due to depletion of adsorbed hydrogen. Similarities in the reaction rates, kinetic parameters, and the stoichiometries of adsorbed hydrocarbon fragments (predicted from kinetic modeling) between the two surfaces suggest that the same reaction mechanism is operative on both surfaces. It was speculated that the reaction occurs through a C_3H_6 intermediate bound as either a metallacyclobutane or a binuclear metallacyclopentane. The similar kinetics observed on the two surfaces suggests that the binding site of

the C_3H_6 intermediate is the same on both Ir(111) and Ir(110)-(1x2). This situation could occur only if the intermediate were located on the (111) facets of the Ir(110)-(1x2) surface, such that the edge atoms of the Ir(110)-(1x2) surface were not involved in the metal-C_3H_6 bond.

For n-butane hydrogenolysis, the major reaction pathways on the two surfaces are clearly different in the linear (T < 475 K) region of the Arrhenius plots shown in Figure 4 [34,35]. The product distributions indicate that the major reaction pathways are $n\text{-}C_4H_{10} + H_2 \rightarrow 2CH_4 + C_2H_6$ on Ir(111) and $n\text{-}C_4H_{10} + H_2 \rightarrow 2C_2H_6$ on Ir(110)-(1x2). In addition, a minor reaction pathway on both surfaces is $n\text{-}C_4H_{10} + H_2 \rightarrow C_3H_8 + CH_4$. The activation energies for n-butane hydrogenolysis are 34 kcal/mole on Ir(111) and 22 kcal/mole on Ir(110)-(1x2). The large differences in selectivity and activation energy between the two surfaces clearly indicate that a different mechanism is operative on the two surfaces.

By using ratio the number of edge (C_7) atoms to the number of (111) face (C_9) atoms (see Figure 5) to define an effective particle size [34,35], the selectivity of n-butane hydrogenolysis as a function of particle size for the two surfaces could be plotted and compared to selectivities measured on supported Ir catalysts [39]. This comparison is shown in figure 6. Clearly, the results on single crystal catalysts correlate well with the results of studies on supported catalysts. In addition, it is clear that high selectivities toward ethane formation are related to the presence of low coordination number surface atoms, i.e., edge atoms. It has been postulated [34,35] that the high

selectivity toward ethane on the Ir(110)-(1x2) surface is the result of hydrogenolysis occuring <u>via</u> a metallacyclopentane intermediate. Thermal decomposition of transition metal metallacyclopentane complexes can result in cleavage of a C-C bond to form two C_2H_4 ligands [40,41]. A similar reaction the Ir(110)-(1x2) surface would likely result in rapid hydrogenation of the resulting adsorbed ethylene molecules due to the large excess of hydrogen present. The open nature of the Ir(110)-(1x2) surface makes it ideally suited for formation of a metallacyclopentane species on the edge (C_7) atoms, while the absence of any edge atoms on the Ir(111) surface makes metallacyclopentane formation sterically unfavorable [34,35]. As a result, ethane formation is favored on Ir(110)-(1x2), while on Ir(111) a different mechanism must operate, which apparently involves cleavage of the terminal C-C bonds to form both methane and ethane.

The hydrogenolysis of neopentane occurs primarily by breaking of a single C-C bond to produce methane and isobutane as the major reaction products [35]. Small amounts of ethane and propane were also produced. The reaction kinetics were similar on the two surfaces, indicating a similar mechanism for both surfaces.

In addition to saturated hydrocarbons, reactions of cyclopropane and methylcyclopropane with hydrogen on Ir(111) and Ir(110)-(1x2) have also been studied [36]. On both surfaces cyclopropane undergoes both hydrogenation to form propane and hydrogenolysis to form ethane and methane. Hydrogenation

dominates below 500 K while hydrogenolysis dominates at higher temperatures. The Ir(110)-(1x2) surface is a factor of three to four times more active that the Ir(111) surface for both reactions. As was the case for n-butane hydrogenolysis, the greater activity for the Ir(110)-(1x2) surface is attributed to higher activity of the low coordination number sites present on this surface [36]. In addition to methane, ethane and propane, propylene production was also observed at high temperatures on Ir(111). Both propylene and propane appear to be formed *via* the same rate limiting step. The onset of propylene production is related to a decrease in the steady-state coverage of hydrogen at high temperatures or under hydrogen-lean conditions, which results in a shift in the selectivity toward the more dehydrogenated product. Propylene production was also observed on Ir(110)-(1x2) under very hydrogen lean conditions.

In contrast to propane hydrogenolysis, the Arrhenius plots for cyclopropane hydrogenolysis on both surfaces exhibit no deviations from linearity over the entire temperature range studied, and the reaction orders in both hydrogen and cyclopropane are essentially zero [36]. These results have been interpreted as indicating that cyclopropane hydrogenolysis occurs by a facile, irreversible ring opening step followed by rate limiting cleavage of a C-C bond in the resulting intermediate [36].

The reaction of methylcyclopropane with hydrogen produced n-C_4 hydrocarbons as the major reaction products on both surfaces [36]. At high temperatures or under hydrogen-lean conditions, n-butene production dominates, while at lower temperatures and

hydrogen-rich conditions, n-butane production dominates. As for cyclopropane, this shift in selectivity is attributed to decreases in the steady-state coverage of hydrogen at high temperatures or under hydrogen-lean conditions. The shift toward n-butene production begins at a higher temperature on Ir(110)-(1x2) than on Ir(111). This difference is due to the higher binding energy of hydrogen on Ir(110)-(1x2) than on Ir(111) [37,38]. Overall, the Ir(110)-(1x2) surface is 3-4 times more active for reaction of cyclopropane with hydrogen than the Ir(111) surface.

ACKNOWLEDGEMENT

We acknowledge with pleasure the partial support of this work by the Department of Energy, Office of Basic Energy Sciences, Division of Chemical Sciences.

REFERENCES

1. J. R. Anderson and B. G. Baker, Proc. Roy. Soc., A271, 402 (1963).
2. P. G. Wright, P. G. Ashmore and C. Kemball, Trans. Far. Soc., 54, 1692 (1958).
3. B. M. W. Trapnell, Trans. Far. Soc., 52, 1618 (1956).
4. M. Salmeron and G. A. Somorjai, J. Phys. Chem., 85, 3835 (1981).
5. T. S. Wittrig, P. D. Szuromi and W. H. Weinberg, J. Chem. Phys., 76, 3305 (1982).
6. P. D. Szuromi, J. R. Engstrom and W. H. Weinberg, J. Chem. Phys., 80, 508 (1984).
7. D. Szuromi, J. R. Engstrom and W. H. Weinberg, Surface Sci., 149, 226 (1985).
8. D. Szuromi, J. R. Engstrom and W. H. Weinberg, J. Phys. Chem., 89, 2497 (1985).
9. J. T. Yates, Jr. and T. E. Madey, Surface Sci., 28, 437 (1971).
10. T. E. Madey, Surface Sci., 29, 571 (1972).
11. T. E. Madey and J. T. Yates, Jr., Surface Sci., 76, 397 (1978).
12. A. V. Hamza, H.-P. Steinruck and R. J. Madix, J. Chem. Phys.. 85, 7494 (1986).
13. A. V. Hamza, H.-P. Steinruck and R. J. Madix, J. Chem. Phys., 86, 6506 (1987).
14. A. V. Hamza and R. J. Madix, Surface Sci., 179, 25 (1987).
15. H.-P. Steinruck, A. V. Hamza and R. J. Madix, Surface Sci., 173, L571 (1986).
16. M. B. Lee, Q. Y. Yang, S. L. Tang and S. T. Ceyer, J. Chem. Phys., 85, 1693 (1986).
17. M. B. Lee, Q. Y. Ceyer and S. T. Ceyer, J. Chem. Phys., 87, 2724 (1987).
18. C. T. Rettner, H. E. Pfnur and D. J. Auerbach, Phys. Rev. Lett., 54, 2716 (1985).
19. C. T. Rettner, H. E. Pfnur and D. J. Auerbach, J. Chem. Phys., 84, 4163 (1986).

20. D. W. Goodman, R. D. Kelley, T. E. Madey, and J. T. Yates, Jr., J. Catal. 64, 479 (1980).
21. D. W. Goodman, Ann. Rev. Phys. Chem., 37 (1986) 425; D. W. Goodman, Accts. Chem. Res., 17, 194 (1984); D. W. Goodman, J. Vac. Sci. Tech., 20, 522(1982).
22. T. P. Beebe, Jr., D. W. Goodman, B. D. Kay and J. T. Yates, Jr., J. Chem. Phys., 87, 2305 (1987).
23. B. D. Kay and M. E. Coltrin, Surface Sci., submitted.
24. B. D. Kay, in preparation.
25. A. V. Hamza, private communication.
26. A. G. Sault and D. W. Goodman, J. Chem Phys., in press.
27. J. T. Carter, J. A. Cusumano, and J. H. Sinfelt, J. Phys. Chem., 70, 2257 (1966).
28. D. J. C. Yates and J. H. Sinfelt, J. Catal. 8, 348 (1967).
29. G. A. Martin, J. Catal., 60, 452 (1979).
30. D. W. Goodman, Surface Sci., 123, L679 (1982).
31. D. W. Goodman, Proceedings of the 8th International Congress on Catalysis, 1984.
32. D. W. Goodman, J. Vac. Sci. Technol., A2, 873 (1984).
33. J. E. A. Clark and J. J. Rooney, Advan. Catalysis, 25, 125 (1976).
34. J. R. Engstrom, D. W. Goodman and W. H. Weinberg, J. Amer. Chem. Soc., 10, 4653 (1986).
35. J. R. Engstrom, D. W. Goodman and W. H. Weinberg, J. Amer. Chem. Soc., submitted.
36. J. R. Engstrom, D. W. Goodman and W. H. Weinberg, in preparation.
37. D. E. Ibbotson, T. S. Wittrig and W. H. Weinberg, J. Chem. Phys., 72 4885 (1980).
38. J. R. Engstrom, T. S. Tsai and W. H. Weinberg, J. Chem. Phys., 87, 3104 (1987).
39. K. Foger and J. R. Anderson, J. Catal., 59, 325 (1979).
40. R. H. Grubbs and A. Miyoshita, J. Amer. Chem. Soc., 100, 1300 (1978).

41. R. H. Grubbs, A. Miyoshita, M. Liu and P. Burk, J. Amer. Chem. Soc., 100. 2418 (1978).

FIGURE CAPTIONS

Figure 1. Comparison of dissociative sticking coefficients of methane on Ni(100) and Ni(111) measured at 1.0 Torr with sticking coefficients predicted from molecular beam data. (From ref. [22])

Figure 2. Comparison of dissociative sticking coefficients of methane, ethane, propane, and n-butane on Ni(100) measured at high pressures with sticking coefficients predicted from molecular beam data. (From ref. [26])

Figure 3. Methane production from ethane hydrogenolysis over Ni(100) and Ni(111) catalysts at total reactant pressures of 100 Torr. H_2/C_2H_6 = 100. (From ref. [30])

Figure 4. Arrhenius plots for n-butane hydrogenolysis on a) Ir(111) and b) Ir(110)-(1x2). (From refs. [34,35] The pressure of n-butane was 1 Torr and that of hydrogen was 100 Torr. The dashed line in a) represents data for n-butane hydrogenolysis on a supported Ir/SiO_2 catalyst [39].

Figure 5. Structural models for the Ir(110)-(1x2) and Ir(111) surfaces. (From ref. [35]) C_n designates the coordinaton numbers of the metal atoms.

Figure 6. Selectivity for ethane production from n-butane hydrogenolysis on iridium as a function of effective particle size. (From refs. [34,35] Also shown are data for n-butane hydrogenolysis on supported Ir catalysts [39]. The temperature is 475 K in all cases.

Comparison of Observed and Beam-Data-Predicted CH_4 Thermal Sticking Coefficients on Ni(100) and Ni(111)

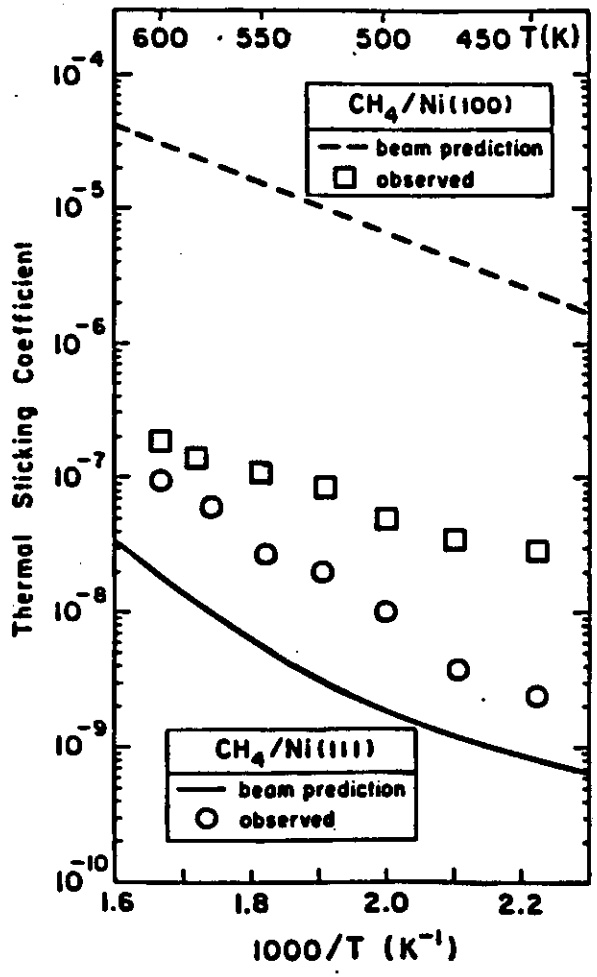

COMPARISON OF MEASURED AND PREDICTED STICKING COEFFICIENTS OF ALKANES ON Ni (100)

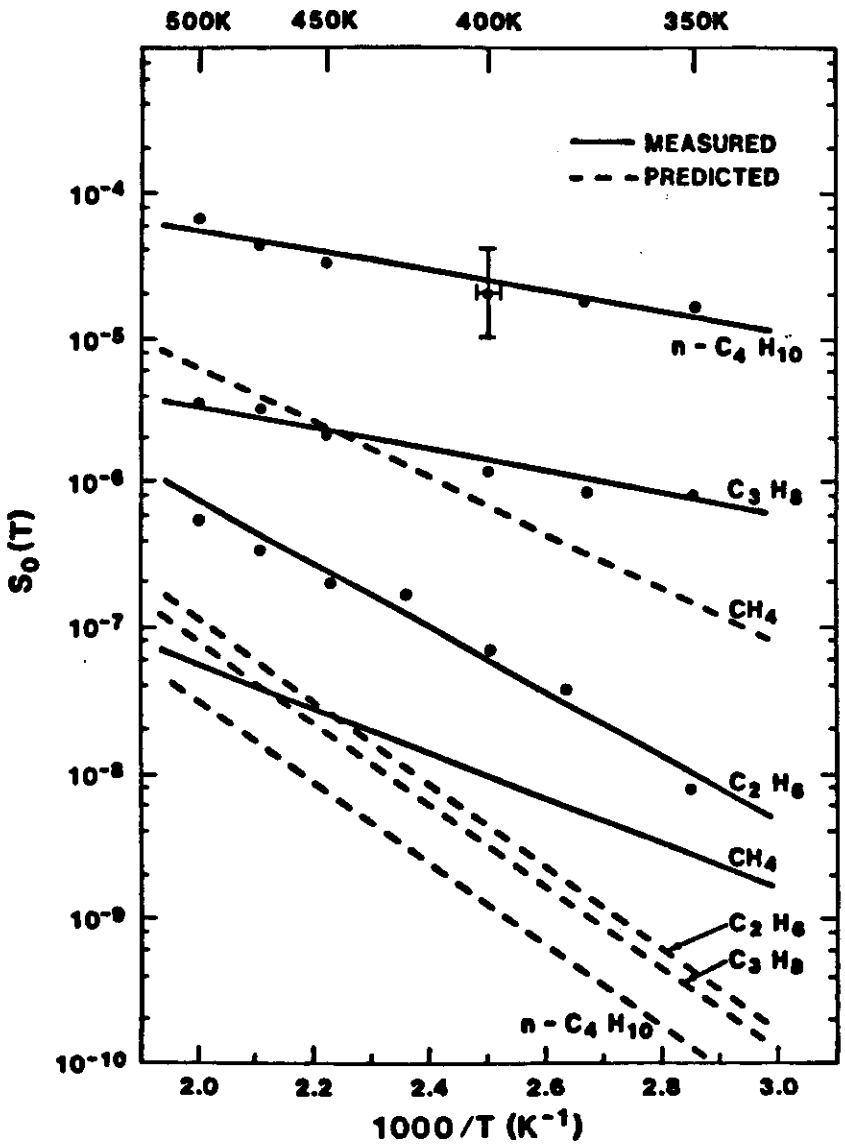

(2)

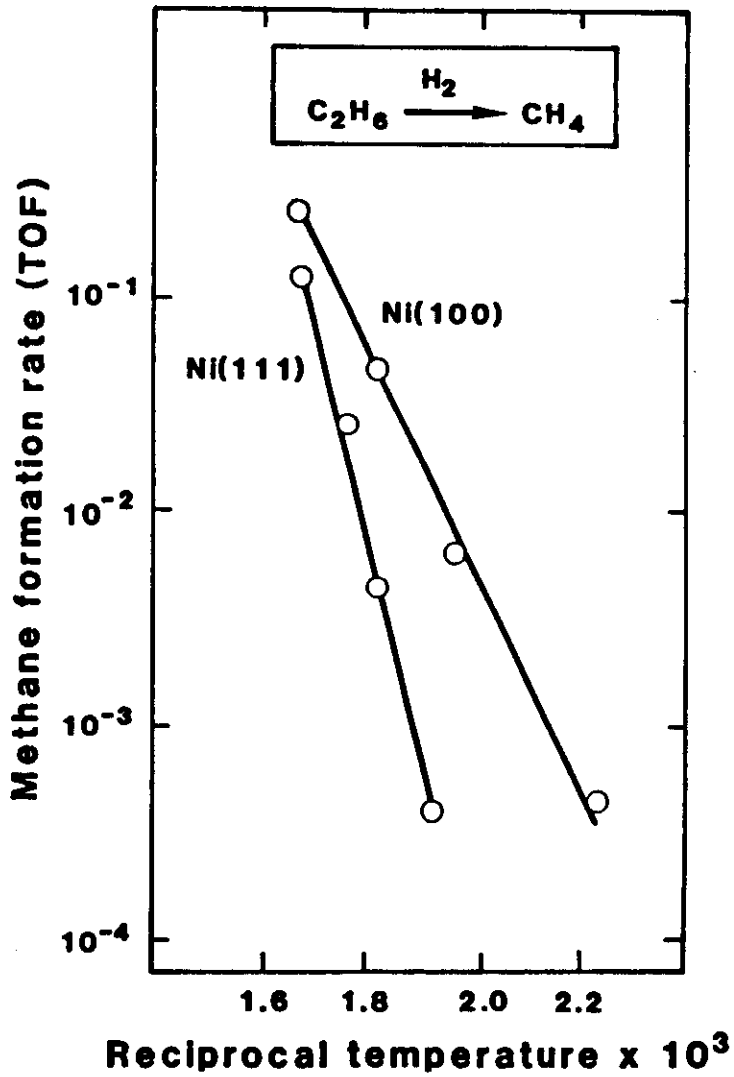

(3)

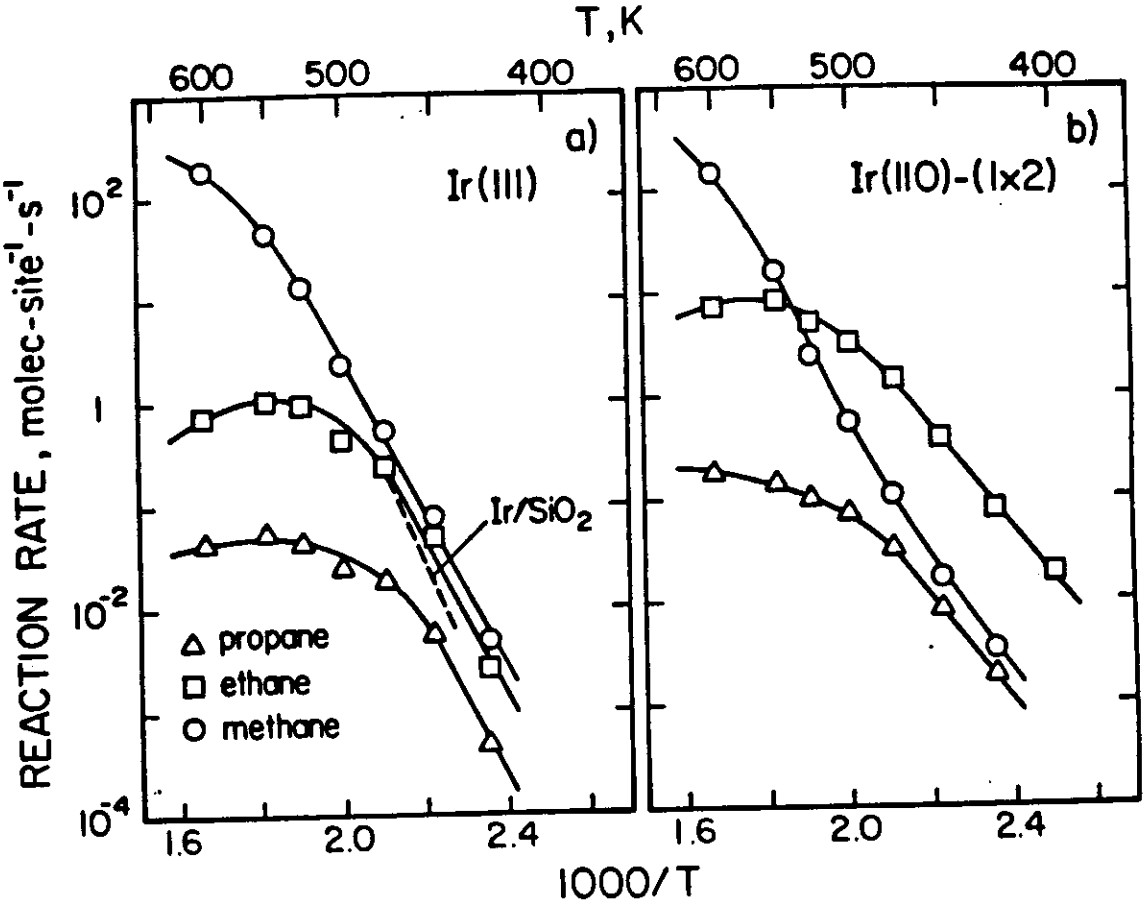
T, K
600
500
400
a)
Ir(111)
b)
Ir(110)-(1x2)
REACTION RATE, molec-site^{-1}-s^{-1}
10^2
1
10^{-2}
10^{-4}
Ir/SiO_2
propane
ethane
methane
1.6
2.0
2.4
1000/T

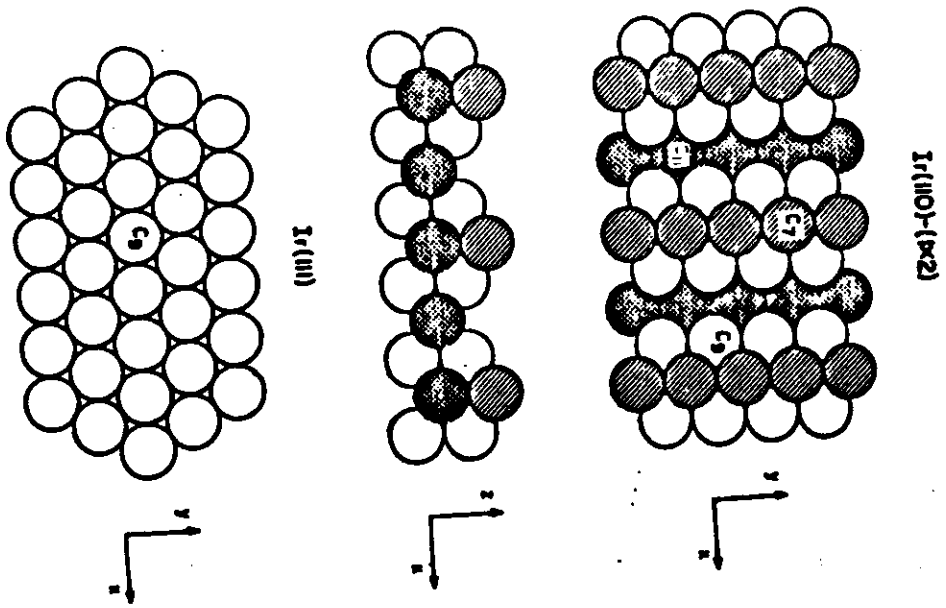
Ir(111)
Ir(110)-(1x2)

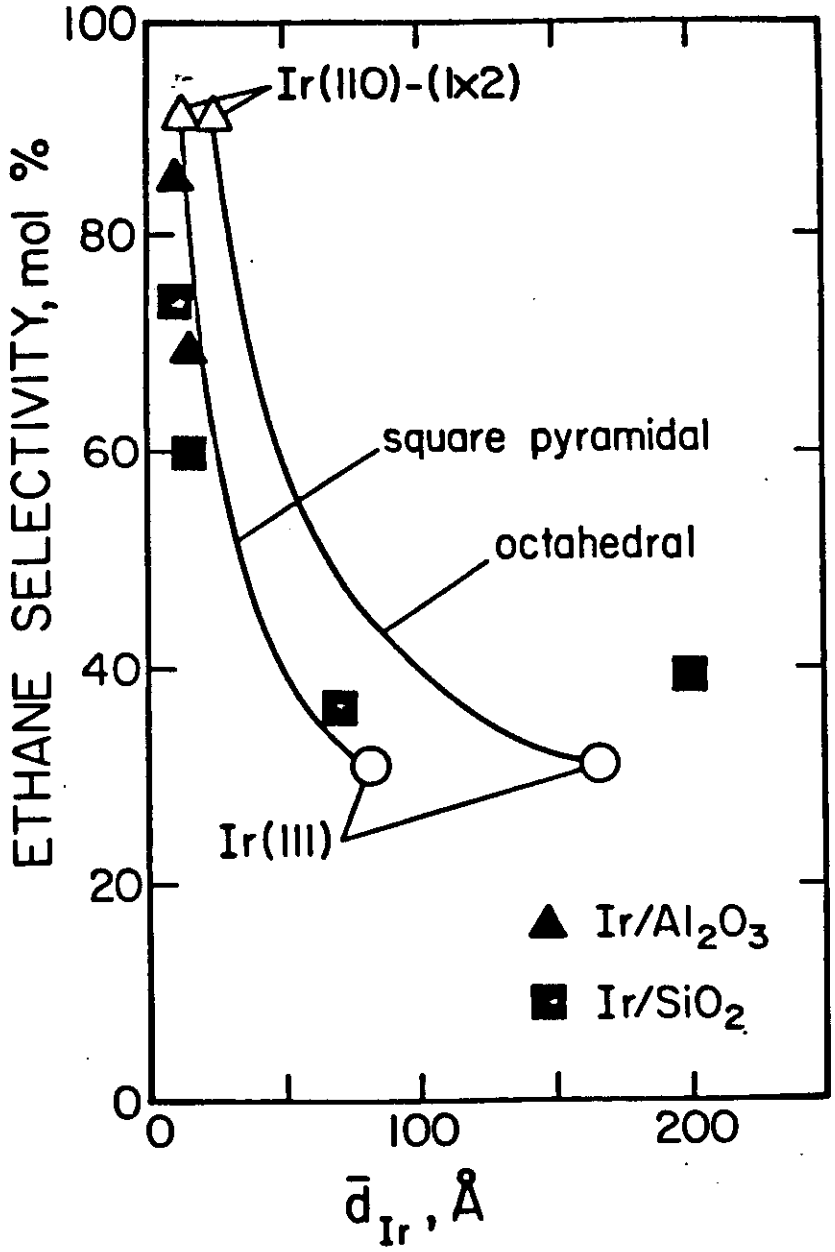
100
80
60
40
20
0
ETHANE SELECTIVITY, mol %
Ir(110)-(1x2)
square pyramidal
octahedral
Ir(111)
▲ Ir/Al2O3
■ Ir/SiO2
0
100
200
d̄Ir, Å

(6)